Title
Molecular recognition of agonist ligands by RXRs

Journal
Molecular Endocrinology, 16(5)

ISSN
0888-8809

Authors
Egea, PF
Mitschler, A
Moras, D

Publication Date
2002

DOI
10.1210/mend.16.5.0823

Peer reviewed

0888-8809/02/$15.00/0
Printed in U.S.A.

Molecular Endocrinology 16(5):987–997

Molecular Recognition of Agonist Ligands by RXRs

PASCAL F. EGEA*, ANDRÉ MITSCHLER, AND DINO MORAS

Laboratoire de Biologie et Génomique Structurales, Institut de Génétique et Biologie Moléculaire et Cellulaire, Centre National de la Recherche Scientifique/Institut National de la Santé et de la Recherche Médicale/Université Louis Pasteur, Parc d'Innovation BP163, 67404 Illkirch cedex, France

The nuclear receptor RXR is an obligate partner in many signal transduction pathways. We report the high-resolution structures of two complexes of the human RXRα ligand-binding domain specifically bound to two different and chemically unrelated agonist compounds: docosa hexaenoic acid, a natural derivative of eicosanoic acid, present in mammalian cells and recently identified as a potential endogenous RXR ligand in the mouse brain, and the synthetic ligand BMS 649. In both structures the RXR-ligand-binding domain forms homodimers and exhibits the active conformation previously observed with 9-*cis*-RA. Analysis of the differences in ligand-protein contacts (predominantly van der Waals forces) and binding cavity geometries and volumes for the several agonist-bound RXR structures clarifies the structural features important for ligand recognition. The L-shaped ligand-binding pocket adapts to the diverse ligands, especially at the level of residue N306, which might thus constitute a new target for drug-design. Despite its highest affinity 9-*cis*-RA displays the lowest number of ligand-protein contacts. These structural results support the idea that docosa hexaenoic acid and related fatty acids could be natural agonists of RXRs and question the real nature of the endogenous ligand(s) in mammalian cells. (*Molecular Endocrinology* 16: 987–997, 2002)

NUCLEAR RECEPTORS (NRs) are important transcriptional regulators involved in widely diverse physiological functions such as embryonic development, cell growth, differentiation and apoptosis, and homeostasis (1). Many of these receptors are regulated by the binding of small hydrophobic ligands such as steroids, retinoids, or thyronines. Some receptors called "orphan receptors" have no (yet) known ligands. In addition, these proteins are important therapeutic targets because a large number of them are implicated in diseases such as cancer, diabetes, metabolic diseases, or hormone resistance syndromes. All NRs share a common functional and structural organization with distinct modules. The E/F region of about 250 amino acids contains the moderately conserved ligand-binding domain (LBD) that carries the ligand-dependent activation function AF2 and is also responsible for the dimerization of the receptor and its interaction with transcriptional coactivators or corepressors (2). Ligand binding triggers major structural changes that affect the position of the C-terminal helix H12 carrying the AF2 activation function (3, 4). Upon agonist binding, the LBD adopts a unique active conformation, the activated receptor being competent for transcriptional coactivator binding.

Retinoids are vitamin A-derived metabolites that play important roles in development, cell growth, differentiation and death, and homeostasis (5). RA pleiotropic effects are transduced by two distinct classes of specific NRs: RARs and RXRs (6). Two natural isomers of RA are high-affinity ligands for these receptors: RXRs bind exclusively the 9-*cis*-isomer (7, 8) whereas RARs interact with both 9-*cis* and all-*trans*-isomers (9, 10). The crystal structures of RXR LBD bound to 9-*cis*-RA (11, 12) illustrated and explained the specificity of this ligand for RXR. Among NRs RXR occupies a central position as an ubiquitous heterodimerization partner with several other NRs such as VDR, PPAR, TR, RAR, and many orphan receptors (13). Although RXRs can be active as homodimers, the RXR heterodimers are the physiologically relevant molecular species (5, 6). Thus, RXR is a key receptor being an obligate partner in many signaling pathways (14).

Three types of RXR heterodimers have been described (13). In some heterodimers (*e.g*. RXR/TR or RXR/VDR) RXR might be a completely silent partner. In others (*e.g*. RXR/RAR), RXR seems to be a conditionally silent partner. In the last category (*e.g*. many RXR/orphan receptors) RXR appears to be a fully active and competent partner. Another property of RXR makes it a special member of the NR superfamily: its propensity to form autorepressed homotetramers in the absence of ligand (15–17).

The sequence homology across the NR superfamily indicates that its members evolved through divergent evolution from a common orphan ancestor. Phylogenetic analysis of NR LBD sequences led to the partition of the superfamily into six subfamilies with several subgroups (18). Interestingly, RARs and RXRs do not belong to the same subfamily. In fact, they appear to be phylogenetically quite distant (32% identity and 51% similarity). RXRs belong to the subfamily that also includes TRs and are also close to ERs that belong to another subfamily (31% identity and 48% similarity). In the RXR subfamily, ultraspiracle protein (USP) is the most closely related to RXR (51% identity and 73% similarity) and appears to be

Abbreviations: DHA, Docosa hexaenoic acid; LBD, ligand-binding domain; LBP, ligand-binding pocket; NR, nuclear receptor; USP, ultraspiracle protein.

the ortholog of RXR in Arthropods (19). RXR binds 9-*cis*-RA from Cnidarians to Vertebrates except in Arthropods where its ortholog is unable to do so. The natural ligand for USP is still unknown, although it was proposed that juvenile hormone, a natural isoprenic compound, could be a candidate (20). The two crystal structures of USP that have been recently reported (21, 22) showed the presence in the binding pocket of an unexpected phospholipidic compound trapped during protein extraction and purification. It is proposed that, during evolution, 9-*cis*-RA binding to RXR occurred very early during metazoan evolution, and the secondary loss was specific to Arthropods for the USP (23).

However, 9-*cis*-RA has been very difficult to detect *in vivo*. Vitamin A (retinol) is acquired via the diet and can be converted into retinal in cells. Retinal is a key metabolite required for the visual process, but also serves as the precursor for all-*trans*-RA biosynthesis. An enzymatic isomerization of the all-*trans*-isomer yields its 9-*cis*-isomer. The regulation of this key enzymatic step controls the relative 9-*cis*/all-*trans* ratio within the cell and therefore regulates the RXR and RAR pathways (24, 25). However, this conversion step remains elusive. The crystal structure of a RXR/RAR LBD mutant heterodimer showed that RXR was also able to bind a fatty acid molecule (26). More recently, docosa hexaenoic acid (DHA or C22:6 all-*cis*-Δ,7,10, 13,16,19), a natural derivative of eicosanoids, has been identified as a new potential ligand for this receptor and was shown to activate RXR in mouse brain cells (27). DHA is abundant in mammalian brain cells, where it can constitute up to 30–50% of the total fatty acids under a predominantly membrane phospholipid-associated form. Interestingly, DHA can be released from phospholipids through PLA_2 and PLC-dependent mechanisms. During late gestation and early postnatal life, DHA becomes highly enriched in the mammalian brain and is required for brain maturation in rodents and humans. DHA accumulates in the retina, a tissue whose development is affected in RXRα-deficient mice (5). DHA deficiency in rats and humans results in abnormalities similar to those observed in RXRγ knock-out mice.

Here we report the crystal structures of human RXR LBD bound to DHA and BMS 649, a synthetic pharmaceutical RXR-selective ligand close to Targretin (LGD1069 from Ligand Pharmaceuticals, Inc., San Diego, CA) and efficiently used in association with the antiestrogen Tamoxifen to treat mammary carcinoma (28).

RESULTS

Structure Determination and Overall Protein Organization

The hRXRα LBD was cocrystallized with the two agonist ligands DHA or BMS 649 in the presence of a synthetic peptide containing a coactivator consensus sequence LXXLL (*Materials and Methods*). The limit of diffraction of these crystals is 1.5 Å but, due to technical limitations, data were collected to 1.9 Å and the structures were solved by molecular replacement using entire and truncated RXR structures as search probes. The data and refinement statistics are summarized in Table 1. The experimental maps showed clear electron densities that could be unambiguously assigned to the ligands.

In all structures, the RXR LBD adopts the canonical conformation of all previously reported agonist-bound NR-LBDs (29), the *trans*-activation C-terminal H12 helix being packed toward the protein core in a hydrophobic groove constituted by helices H3, H5, and H11 (Fig. 1, A and B). To stabilize the active conformation, crystallization trials were carried out in the presence of a synthetic peptide containing the consensus sequence LXXLL, which mimics the NR-interacting motif (30–32). In the structure, the coactivator peptide is tightly bound to the LBD AF-2 surface formed by helices H3, H4, and H12 of the LBD. The polar and hydrophobic interactions between the receptor and the coactivator peptide are similar to those previously described in other LBD-coactivator peptide complex structures (30–32).

The Homodimeric Association Mode of Agonist-Bound RXR LBD and the Dimerization Interface

In contrast to the situation of holo-RXR LBD bound to 9-*cis*-RA in the absence of coactivator peptide where a monomeric form of the complex was observed (11), all the present structures show a homodimeric association mode for agonist-bound RXR LBD in the presence of the coactivator peptide. Although in the tetragonal crystals of both RXR-DHA and RXR-BMS 649 complexes, the asymmetric unit contains a single monomer, the previously described biological homodimer is rebuilt through the space-group symmetry operators. Comparison with the previously reported homodimeric structures of *apo*-RXR (33) or heterodimeric structures of RXR/RAR (26) or RXR/PPAR (12) shows that the overall dimeric arrangement is identical (Fig. 1C). The present results based on these crystallographic structures are in agreement with extensive biophysical studies carried out on RXR, RAR, and VDR LBDs in solution by small-angle x-ray and neutron scattering and analytical ultracentrifugation that unambiguously demonstrated that holo-RXR LBD was a dimer in solution regardless of protein concentration (17, 34). In the case of the RXR-BMS 649 complex, a triclinic crystal form was also obtained in the same crystallization conditions. In this specific case the asymmetric unit contains two LBD homodimers weakly associated into a tetramer through the H1 helices. This crystal packing-induced tetramer is not reminiscent of that previously reported for the *apo*-RXR LBD (16, 17).

Using the same crystallization conditions, notably the presence of coactivator peptide, we also were able to grow isomorphous tetragonal crystals of RXR LBD in the presence of 9-*cis*-RA. Furthermore, in the absence of peptide we also grew crystals of the RXR-BMS 649

Table 1. Data Collection and Statistics of Crystallographic Data and Refinement

Data Sets	DHA (Tetragonal)	BMS 649 (Tetragonal)	BMS 649 (Triclinic)
Resolution (last shell) (Å)	30–1.9 (2.0–1.9)	30–1.9 (2.0–1.9)	30–2.0 (2.1–2.0)
Total reflections	99,469	81,070	194,870
Unique reflections	19,305	19,091	79,918
Redundancy	5.2	4.2	2.4
Completeness (last shell) (%)	98.8 (96.6)	98.7 (93.5)	95.9 (96.6)
Rsym[a] (last shell) (%)	4.6 (11.5)	7.6 (9.3)	6.3 (12.4)
I/σ(I) (last shell)	24.9 (11.3)	18.4 (9.3)	15.6 (7.9)
Refinement statistics			
Reflections in working set (92.5% at 2 σ)	16,884	17,234	71,161
Reflections in test set (7.5% at 2 σ)	1,337	1,354	5,850
R_{cryst}[b] (%)	20.1	20.1	19.5
R_{free}[b] (%)	24.9	22.8	23.2
r.m.s.d. bonds (Å)	0.0055	0.0057	0.0061
r.m.s.d. angles (degrees)	1.173	1.165	1.167
Nonhydrogen protein atoms[c]	1,791	1,772	1,853 1,772 1,853 1,772
Nonhydrogen ligand atoms[c]	24	28	28 28 28 28
Solvent molecules	243	199	829
Average B factor (Å^2)	27.9	26.0	25.3
Nonhydrogen protein atoms[c]	25.8	30.4	22.3 28.3 22.4 28.3
Nonhydrogen ligand atoms[c]	37.1	14.5	14.7 20.9 14.6 20.9
Solvent molecules	40.9	37.5	38.8

r.m.s.d is the root-mean square deviation from ideal geometry.

[a] $R_{sym} = \Sigma hkl\ \Sigma i\ |I\ hkl,i - \langle I\ hk,i\rangle|/\Sigma hkl\ \Sigma i\ |I\ hkl,i|$ where $\langle I\ hk,i\rangle$ is the average intensity of the multiple hkl, i observations for symmetry-related reflections.

[b] $R_{cryst/free} = \Sigma|F_{obs} - F_{calc}|/\Sigma|F_{obs}|$. F_{obs} and F_{calc} are observed and calculated structure factors, R_{free} is calculated from a randomly chosen 7.5% of reflections (2σ), and R_{cryst} is calculated for the remaining 92.5% of reflections (2σ).

[c] In the triclinic form the two homodimers are constituted with monomers 1 and 2, and 3 and 4, respectively.

complex isomorphous to those described for the RXR-9-*cis*-RA (35). A close inspection of the packing contacts in the various crystal forms provides a likely explanation for the oligomeric state fluctuations. In the absence of the peptide (monomeric case), the hydrophobic groove formed by helices H3, H4, and H12 that constitutes the target of the LXXLL motif is filled with hydrophobic peptides of related sequence of neighboring molecules (11). The saturation of the hydrophobic groove is required to stabilize the crystal packing (36, 37) but cannot be obtained without disrupting the homodimeric units. Although in solution the monomer-dimer equilibrium is strongly in favor of the second entity, the crystal that competes for the monomers will find enough material if the packing energy is close to that provided by the dimeric association. The comparison of the surface buried upon association provides a reasonable estimate of the energy involved. In the present homodimers the dimerization interface is about 1,100 $\pm$ 20 Å^2. The bound coactivator peptide releases the constraint by filling the hydrophobic groove and allowing different packings.

The Ligand-Binding Pockets (LBPs)

DHA and BMS 649 molecules are buried in the predominantly hydrophobic pocket that was identified in RXR-9-*cis*-RA complexes (11, 12). Despite the overall similarity of protein-ligand interactions, some differences can be noted. Additional residues, such as V265 on H3, I310 on H5, I324 on the β-strand, and V346 on H7, interact with either DHA or BMS 649 whereas they are not in contact with 9-*cis*-RA. In contrast with the case of the RXR-9-*cis*-RA holostructure, all atoms of both DHA and BMS 649 ligands are in direct van der Waals contact with the protein. Thus, the majority of protein-ligand contacts are van der Waals interactions (Fig. 2A, B, and C). The elongated and L-shaped binding pocket is sealed by R316 of helix H5 on one side and transactivation helix H12 on the other side. Both DHA and BMS 649 contain a carboxylate group that is involved in an ionic interaction with the strictly conserved basic residue R316 of helix H5 and forms a hydrogen bond with the backbone carbonyl amide group of the β-turn residue A327. These two anchoring interactions are observed in all the holostructures of RXRs or RARs that have been solved. The carboxylate moiety also participates in a water-mediated hydrogen bond network involving the backbone carbonyl group of L309 and the side chains of Q275 and R371. As in the case of the RXR-9-*cis*-RA holostructure, no interaction is established between ligands and the transactivation helix H12.

In both structures (Fig. 2, D and E) the ligand molecules adopt a well defined conformation as shown by the clearly defined electron density and the average B factors values, respectively, of 37 Å^2 and 14 Å^2 observed for ligand atoms of DHA and BMS 649 (Table 1). The respective conformational rigidity of the ligands accounts for the difference. Indeed, the DHA molecule

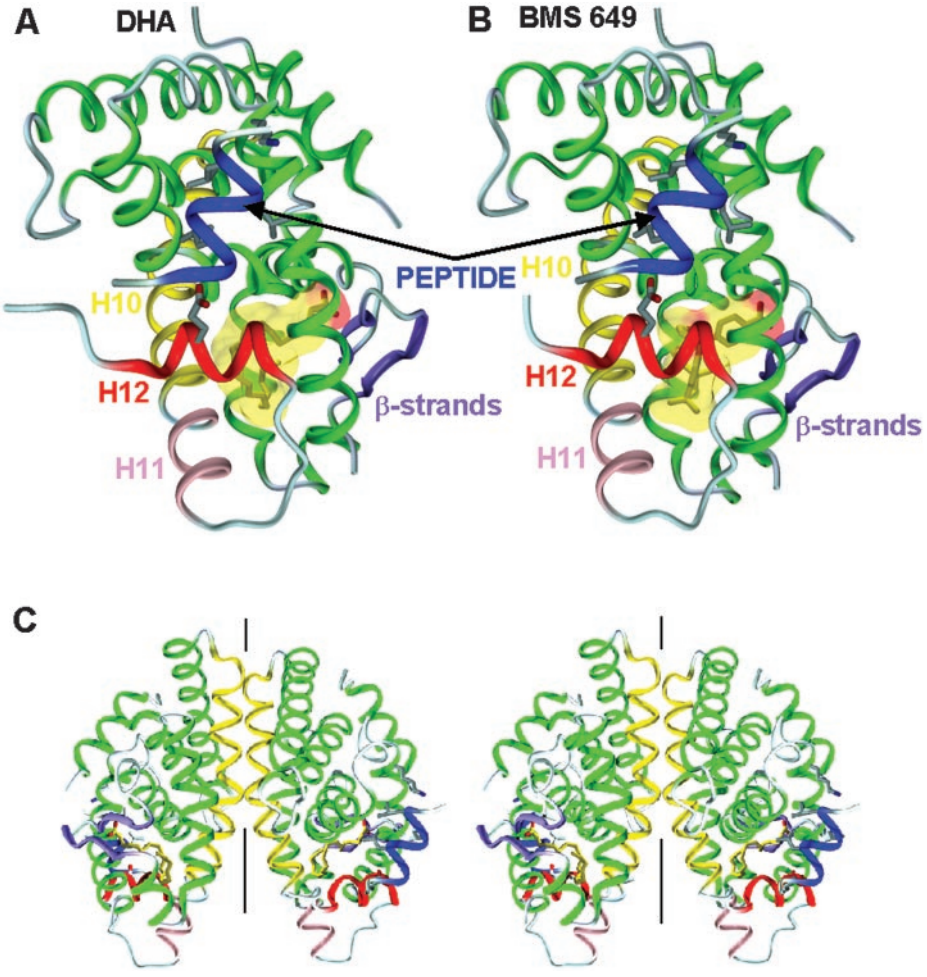

Fig. 1. The Structures of the RXR LBD Bound to DHA or BMS 649 Compounds and a Coactivator Peptide

The RXR-DHA (A) and RXR-BMS 649 (B) complex structures and a stereoview of the homodimeric association mode of agonist bound holo-RXR LBD (C) are shown. The crystallographic symmetry 2-fold axis is indicated with a *line*. Helices H10, H11, and H12 are colored in *yellow, pink*, and *red,* respectively. The coactivator helical peptide is drawn in *blue*. The ligand molecules of DHA and BMS 649 are displayed in *yellow* and *red* for their carbon and oxygen atoms, respectively.

is much more flexible than the rigid and constrained BMS 649 compound. The 9-*cis*-RA molecule represents an intermediate case in terms of rigidity and conformational flexibility. In particular, all three ligands interact extensively with a set of residues delineating the binding cavity. This set includes residues A271,Q275 (both on H3), L326 (on the β-strand), and F313 (on H5) at the entrance of the LBP and residues I268 (on H3) and C432 (on H11) at the level of the hinge and at the bottom of the L-shaped binding cavity.

The solvent-accessible surfaces of the ligand binding cavities and their occupancy reveal specific features of the ligand recognition by RXR (Fig. 3). As shown in Table 2, compared with 9-*cis*-RA, BMS 649 and DHA are larger molecules with molecular volumes of 364, 413, and 427 Å^3, respectively; nevertheless, the solvent-accessible volume of the binding cavity in the BMS 649 complex is about 476 Å^3 and is thus significantly lower than the value of 528 Å^3 calculated in the DHA complex (as a comparison, this value is 504 Å^3 in the 9-*cis*-RA complex). This 10% amplitude decrease in LBP volume is mainly due to the reorientation of a single residue, the side chain of residue N306 on helix H5 that moves its polar amide group from a surface-exposed position observed in both the 9-*cis*-RA and DHA complexes (Fig. 2C) to a buried position inside the pocket in the BMS 649 complex (Fig. 2D).

The calculated values show a clear correlation between the protein-ligand contacts and the occupancy ratio of the LBPs (Table 2). A similar number of 95 and 97 protein-ligand contacts are observed in both DHA and BMS 649 complexes, respectively, compared with the significantly lower number of 77 contacts observed for the 9-*cis*-RA complex. Concomitantly, we observe a remarkable increase in the LBP occupancy ratios by the different agonists that ranges from 72% for 9-*cis*-RA to 80% and 88% for DHA and BMS 649, respectively.

The adaptability of RXR ligands is revealed by the superimposition of the corresponding LBPs that

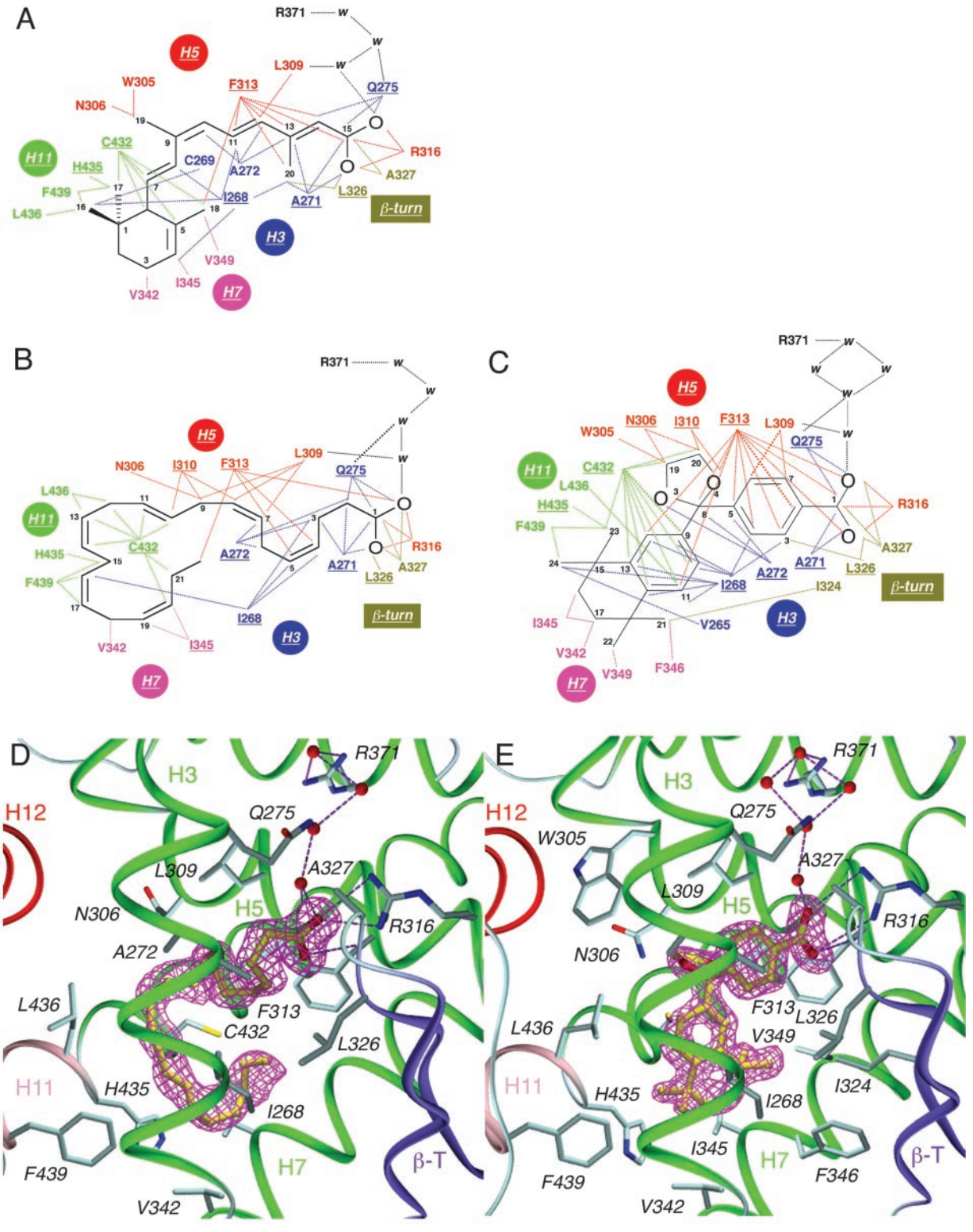

Fig. 2. The LBPs of RXR/DHA and RXR/BMS 649 Complexes

A–C, Schematic drawing showing the interactions between the protein and the ligand molecules: 9-*cis*-RA (A) (11), DHA (B), and BMS 649 (C). Only contacts closer than 4.2 Å are indicated with *dotted lines*. Residues in close contact (< 3.7 Å) are *underlined*. The DHA (D) and BMS 649 (E) molecules are shown in their *Fo-Fc* electron density omit maps contoured at 3.0 and 2.5 σ, respectively. Water molecules are indicated as *red spheres*. Direct or water-mediated hydrogen bonds are depicted as *magenta dotted lines*. Only residues closer than 4.2 Å are shown.

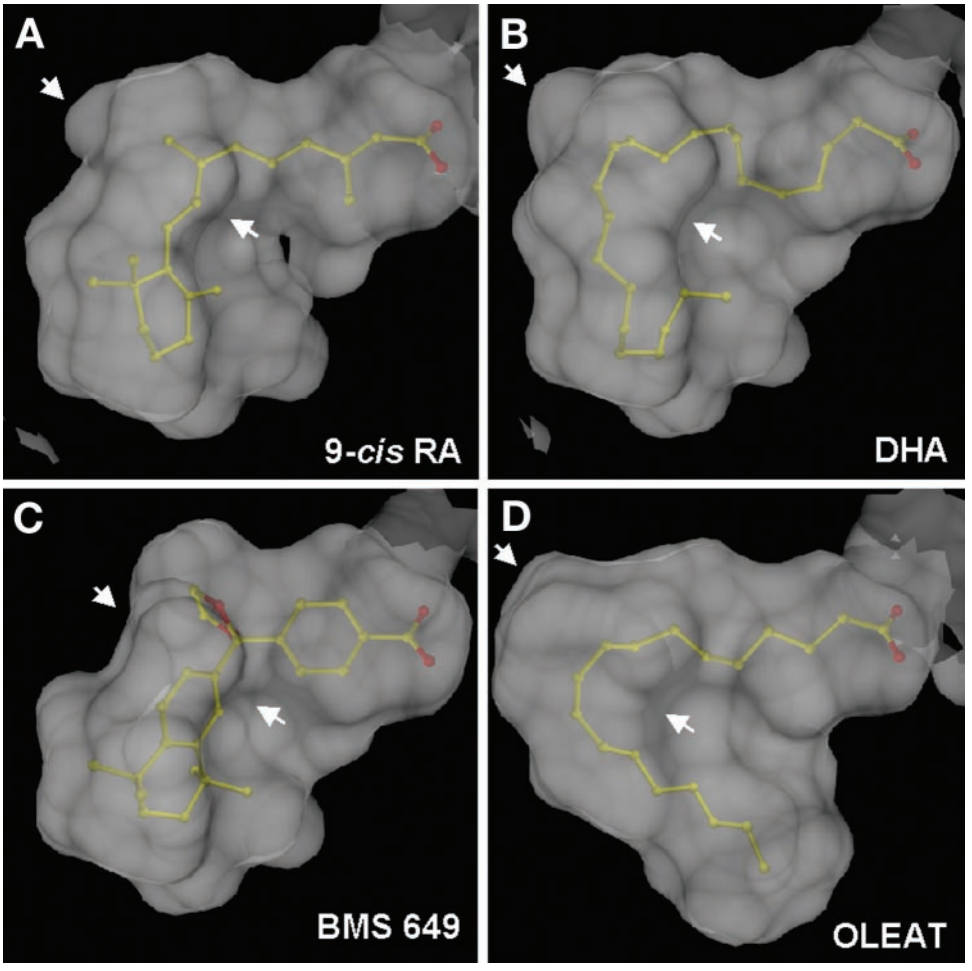

Fig. 3. Comparison of Solvent-Accessible Surfaces in the LBPs of Several RXR/Ligand Complexes

Solvent-accessible surfaces computed with the MSMS program are displayed with *DINO* (59) as *gray* transparent envelopes. The ligands 9-*cis*-RA (A) (11), DHA (B), BMS 649 (C), and oleic acid (D) (26) are shown by transparency. The *arrows* indicate the hinge region of the L-shaped binding pocket.

shows the conserved structural features of ligand recognition by RXR (Fig. 4). The position of the carboxylic group is remarkably stable within the three-agonist structures. The hydrophobic channel at the H3/H5 end of the cavity is particularly tight. With the BMS 649 molecule, the benzoate group optimally occupies this part of the binding cavity. The β-ionone ring binding subpocket (delineated by helices H3, H7, and H11, as defined in the 9-*cis*-RA complex), is an exclusively hydrophobic cavity that is fully occupied by DHA (ligand atoms C14-C22) or by BMS 649 (the tetra hydro tetramethyl naptho group). At the level of the hinge of the L-shaped binding pocket, the situation is different: BMS 649 occupies this corner more efficiently due to the above mentioned motion of the side chain of residue N306. The solvent-accessible volumes of the LBPs reveal empty cavities around residues W305/N306 (on helix H5) and residues I268/F313 (on helices H3 and H5,respectively). These cavities were observed when we first reported the RXR-9-*cis*-RA complex structure (11), and these two new agonist complex structures highlight the structural determinants of the molecular specificity of RXRs toward agonist ligands. This hinge region, where these two cavities are located, appears to be the region of maximal flexibility and adaptability within the RXR LBP.

DISCUSSION

Since the initial discovery of 9-*cis*-RA as a high-affinity ligand for RXR, two monocyclic terpenoid compounds, methoprenic acid (38) and phytanic acid (39, 40), have also been identified as RXR ligands (Fig. 5). Unlike 9-*cis*-RA, which also activates RARs, these two noncyclic terpenoids are highly selective for binding and activation of RXRs, albeit at much higher concentrations than 9-*cis*-RA. Methoprenic acid is a metabolite of the pesticide methoprene, a synthetic analog of the juvenile hormone, an insect growth regulator. Phytanic acid is a metabolite of phytol, a chlorophyll de-

Table 2. Comparison of the Binding Pocket Properties in RXR-Agonist Ligands Complexes

Protein/Ligand	Ligand Volume	Cavity Volume	Cavity Occupancy	Contact No. Total (vdw/polar)	Average Distance (vdw/polar)	Dissociation Constant
RXR/9-*cis*-RA						~2 nM
RXR[a]	364 Å^3	494 Å^3	73%	77 (71/6)	3.8/3.0	
RXR/PPAR[b]	364 Å^3	513 Å^3	71%	77 (71/6)	3.8/3.2	
RXR/DHA[c]	427 Å^3	528 Å^3	80%	95 (89/6)	3.8/3.0	~50–100 μM
RXR/BMS 649[d]						~5–10 nM
Tetragonal	413 Å^3	480 Å^3	86%	95 (89/6)	3.8/3.2	
Triclinic	413 Å^3	472 Å^3	88%	99 (92/7)	3.8/3.2	
RAR/9-*cis*-RA[e]	364 Å^3	430 Å^3	84%	92 (84/8)	3.9/3.3	~1 nM

Ligand volumes were calculated using the *MSMS* program. Cavity volumes were computed with the *VOIDOO program* (58). Occupancy is defined as the ratio between the ligand volume and the cavity volume. All protein ligand contacts including polar contacts (hydrogen bonds) and van der Waals (vdw) contacts (with a distance cutoff of 4.2 Å) were evaluated using the *CCP4* suite of programs.

[a] and [b], Two RXR/9-*cis*-RA complex crystal structures are available, the crystal structure of RXR bound to 9-*cis*-RA (11) and the crystal structure of a RXR/PPAR heterodimer with 9-*cis*-RA bound in the RXR subunit (12).

[c] and [d], The RXR/DHA and RXR/BMS 649 complexes are described in this study.

[e] The RAR/9-*cis*-RA structure has been described in the previously reported structure of RAR bound to 9-*cis*-RA (49).

The RXR/oleat structure has been described in the previously reported structure of a RXR/RAR heterodimer (26). In this latter structure, RXR adopts an antagonist conformation.

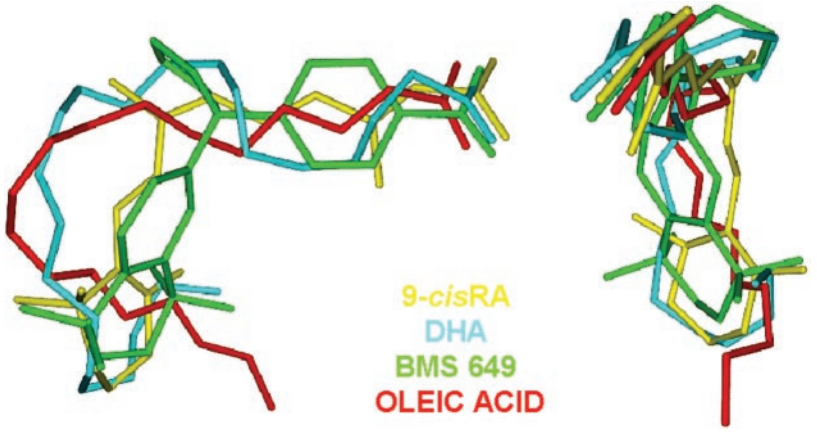

Fig. 4. Comparison of Ligand Positioning in RXR Binding Pocket Reveals a Conserved Set of Molecular Features in RXR-Ligand Recognition

The relative orientation and positioning of ligands is presented after superimposition of the protein structures: 9-*cis*-RA (11), DHA, BMS 649, and oleic acid (26) are depicted in *yellow, cyan, green,* and *red,* respectively.

rivative obtained in the diet. Several severe diseases, such as Refsum's disease and Zellweger's syndrome or neonatal adrenoleukodystrophy, are associated with the inability to catabolize phytanic acid. A simple docking exercise reveals that these molecules can easily adapt to the RXR LBP, but will not fully occupy the cavity. Furthermore, the recent structure of RXR/RAR heterodimer (18) showed the unexpected presence of an oleic acid molecule, a mono unsaturated fatty acid with 18 carbon atoms, in the RXR binding pocket; this fatty acid has been shown to be a partial agonist in *in vitro* transcriptional assays. Similarly, in the case of the orphan receptor RA-related receptor, as observed for the RXR/RAR heterodimer, the crystal structure of this receptor revealed the presence of a fatty acid molecule identified as stearic acid, a saturated fatty acid with 18 carbon atoms (29). It has been suggested that the ability of RXR to bind fatty acid molecules may underline the potential involvement of RXR in the lipid homeostasis through complex feedback mechanisms in potential association with other NRs (such as PPAR or Farnesoid X receptor).

A similar observation can be made in the case of PPARs. PPARα and PPARγ bind eicosanoids, polyunsaturated lipids derived from arachidonic acid metabolism (41) such as leukotrienes (*e.g*. leukotriene B_4) (42) or PGs (*e.g*. 15-deoxy-Δ12,14-PGJ_2) (43, 44). In the case of PPARs, various fatty acids including those that vary in both chain length and degree of saturation bind and activate the PPARs at physiological concentrations. Given the established roles of PPARs in lipid and glucid homeostasis, it is suggested that fatty acids or their metabolites are natural PPAR ligands and exert a feedback regulation. Structural analyses of

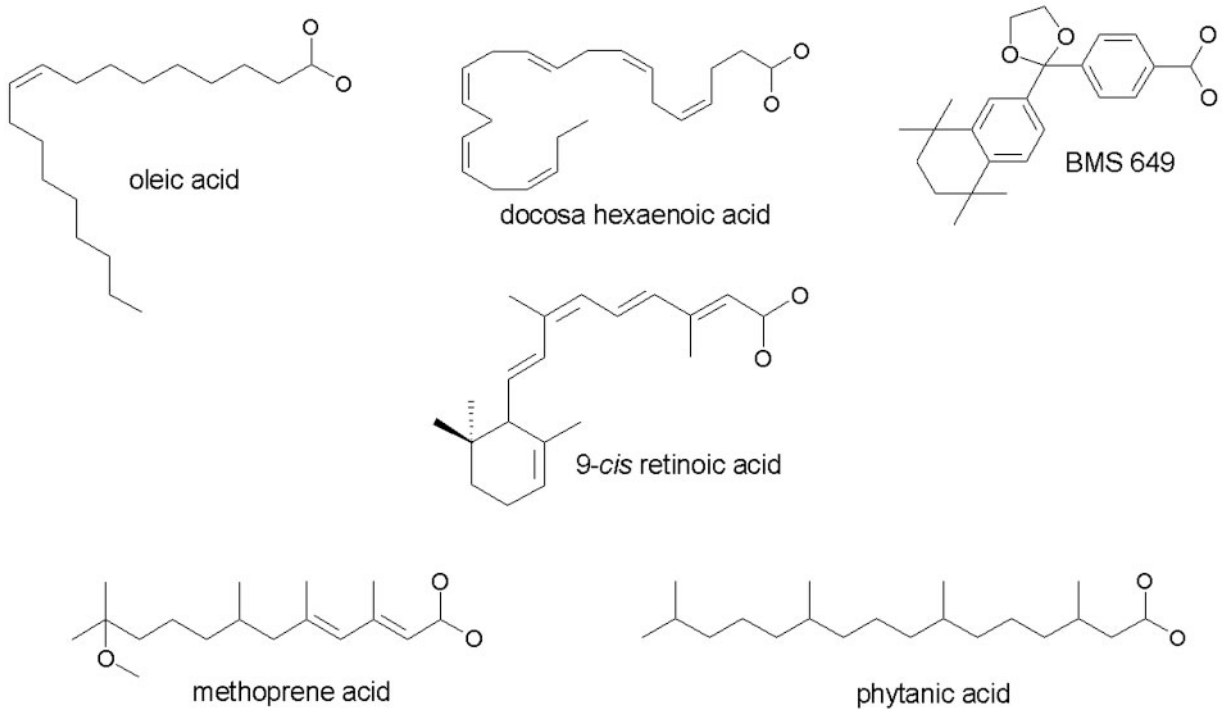

Fig. 5. Schematic Structures of Identified RXR Ligands, 9-*cis*-RA, Oleic Acid, Docosa Hexaenoic Acid, BMS 649, Methoprene Acid, and Phytanic Acid

PPARγ and β/δ LBDs reveal that their binding pockets are about three to four times larger than those of other NRs; they are sufficiently large to allow different fatty acids to bind in multiple conformations (45). These findings suggested that PPARs might have evolved to function as lipid sensors and recognize a number of different metabolites rather than a single high-affinity hormone. Therefore, it appears that flexible saturated or unsaturated fatty acids are probably physiologically relevant ligands of many NRs (RXRs, PPARs, and orphan receptors) even if they display lower affinity and activity compared with other compounds. Local high cellular concentrations could compensate their rather low affinity toward RXRs.

The RXR-DHA complex structure shows how the binding pocket is well ordered around the ligand molecule, optimizing protein-ligand contacts and ensuring a specific molecular recognition (Fig. 2D). Indeed, RXR activation by DHA was shown to be sensitive to mutations altering ligand-binding specificity (27, 46, 47). Furthermore, DHA fails to activate other NRs such as TR, VDR, and RAR (27). This is quite remarkable because 9-*cis*-RA binds to both RXRs and RARs but under two subtly different conformations (11). Observation of the RAR LBP shows that it would be impossible for the flexible, but too long, DHA molecule to fit in. As in the case of PPARs, other polyunsaturated fatty acids closely related to DHA such as docosa tetraenoic acid (C22: 4 all-*cis*-Δ7,10,13,16) or arachidonic acid (C20: 4 all-*cis*-Δ5,8,11,14) can activate RXRs but with lower efficiency; on the other hand, other fatty acids such as erucic acid (C20: 1-*cis*-Δ13) fail to activate RXRs (27). The comparison of RXR *vs.* RAR specificity toward retinoids and eicosanoids illustrates the role of the NR LBP overall geometry in the process of molecular recognition of a specific class of ligands.

The RXR-BMS 649 complex shows that the protein can undergo a small, but significant, conformational fluctuation while maintaining all other contact points of the LBP. The reorientation of one single side-chain residue (N306) is sufficient to reduce the volume of the cavity up to 10% but does not affect the position of any other atom of the pocket. This side chain motion that generates additional stabilizing contacts is most probably the result of an attraction by the partial negative charge of the ligand oxygen atoms (Fig. 5). An artifact due to crystal packing can be excluded because the conformation is identical in the two nonisomorphous crystal forms of the RXR-BMS 649 complex and different in the isomorphous crystals of the DHA complex. As a result of the change of volume, the level of occupancy of the LBP by the BMS 649 ligand is the highest observed so far.

Why, despite a smaller number of protein-ligand contacts, does 9-*cis*-RA exhibit a higher affinity toward RXR than DHA, BMS 649, or oleic acid? The affinity between the receptor and its ligand results from the energy balance between the cost associated with the desolvation and the conformational adaptation of the bound ligand and the gain resulting from the contacts established within the pocket. This has been described in the case of

the structures of VDR-superagonist complexes (48). The RXR-9-*cis*-RA complex may thus represent an optimal compromise between an energetically favorable ligand conformation and sufficient protein-ligand contacts.

Concluding Remarks

The RXR agonists analyzed in this work exhibit a striking structural resemblance with 9-*cis*-RA, as their intrinsic flexibility (*e.g.* DHA) or their structural adequacy (*e.g.* BMS 649) allow them to fit into the hydrophobic LBP (Fig. 4). Thus, the hypothesis that ligands adapt their conformation to the binding pocket as was shown in the case of RAR-agonist (49, 50) and VDR-superagonist complexes (48) is also valid in the case of RXRs. The mechanism of protein-ligand recognition is a mutual induced fit that leads to an essentially unique conformation of the LBD.

In contrast to the situation in RARs, the three RXR isotypes (α, β, and γ) exhibit a strict conservation of all the amino acids delineating the binding pocket. Thus, for generating RXR isotype-specific compounds, ligands would probably have to reach residues outside the pocket. This second shell of residues could be made accessible through induced conformational changes affecting the LBP (*i.e.* at the level of the residue N306) as revealed by the structure of the RXR-BMS649 complex. Although this hypothesis can be questioned, the role of the second shell of residues delineating the binding pockets of proteins has been extensively studied, especially in the case of human immunodeficiency virus type 1 protease-inhibitor complexes (51, 52). Such residues have been shown to play a role in the protein-ligand interactions both at the level of affinity and specificity.

In summary, all physiological, genetic, biochemical, and structural data suggest that RXR could be an opportunistic NR that can bind, with differential affinity and transcriptional activity, several ligands such as 9-*cis*-RA or fatty acids derived from arachidonic acid metabolism depending on the cellular and metabolic context and the local concentration and supply in each potential ligand. Thus, RXR, alone or in association with a heterodimeric partner, could act as a metabolite intracellular sensor.

MATERIALS AND METHODS

Protein Expression and Purification

The human RXRα LBD (residues Thr223 to Thr462) was cloned as an N-terminal hexahistidine-tagged fusion protein in pET15b expression vector and overproduced in *Escherichia coli* BL21 (DE3) strain. Cells were grown in 2× LB medium and subsequently induced for 5–7 h with 0.8 mM isopropyl-β-D-thiogalactopyranoside at 20 C. In contrast with the previously reported purification of RXRα LBD-9-*cis*-RA complex (35), we purified the apoprotein. Purification procedure included an affinity chromatography step on a cobalt-chelating resin followed by preparative gel filtration to remove apo-tetrameric RXRα LBD species and to keep only the apohomodimer species of RXRα LBD (17). After tag removal by thrombin digestion, protein was further purified on an analytical gel filtration. Apoprotein was concentrated and incubated with a 9:1-fold excess of ligand (alcoholic solutions of DHA or BMS 649) and a 3:1-fold excess of synthetic peptide harboring the second GRIP1 NR-box (30) KHKILHRLLQDSS. Because of ligand photosensitivity, all further manipulations were carried out in dimmed light. Purity and homogeneity of RXRα LBD-ligand complex were assessed by SDS and native PAGE and denaturant and native electrospray ionization mass spectrometry.

Crystallization

Crystals of hRXRα LBD-ligand-peptide complexes were obtained at 22 C and 4 C using vapor diffusion technique in hanging and sitting drops. Reservoir solutions contained 100 mM piperazine-*N,N′*-bis-(2-ethanesulfonic acid), pH 7.0, or bis-Tris, pH 6.5, 5–20% PEG4000, and 5–20% glycerol. Crystals with DHA were easier to obtain and single monocrystals could be grown at 22 C by spontaneous nucleation. By contrast, crystals with BMS 649 appeared to be more fragile and were exclusively grown at 4 C. These crystals belong to the tetragonal space group $P4_32_12$ with unit cell parameters a = b = 64.4 Å, c = 111.4–112.8 Å, for DHA and BMS 649 complexes, respectively, with one monomer per asymmetric unit and a solvent content of 47%. In the case of the crystals with BMS 649, two crystal forms were simultaneously observed in the same crystallization drops: the tetragonal form and a triclinic form with unit cell parameters a = 47.1 Å, b = 64.7 Å, c = 94.8 Å, and α = 110.0° angle, β = 92.9° angle, γ = 90.0° angle with two homodimers per asymmetric unit and a solvent content of 45%.

Data Collection, Structure Determination, and Refinement

Crystals were flash frozen in liquid ethane using the reservoir solution containing 25% glycerol as a cryoprotectant. One single native data set was collected for each complex on beam line ID14-EH1 at the European Synchrotron Radiation Facility (Grenoble, France). For all complexes and crystal forms, crystals diffracted to at least 1.9Å. Data were processed using DENZO and SCALEPACK programs (53). The structures were solved by molecular replacement using three model probes: the entire or H11-H12 truncated holo wild-type RXRαLBD monomer bound to the natural agonist 9-*cis*-RA (11) and the entire holo-F313A mutant RXRα LBD monomer bound to oleic acid (26). Molecular replacement calculations were carried out on the tetragonal form data sets between 30 and 3.5 Å using the AmoRe program (54). All models gave unambiguous solutions, the best model being the truncated agonist bound holostructure with a correlation coefficient of 37.8% and an R-factor of 48% after fast rigid body refinement. The first map allowed an unambiguous modeling of the coactivator peptide and the repositioning and rebuilding of helix H12 and H11-H12 loop. Iterative cycles of rigid body refinement and torsion angle molecular dynamics at 5,000 K in *CNS* (55) interspersed with model building in *O6* (56) yielded the complete structures. Although their electron densities were clear, the ligand molecules were only included at the last stages of the refinement. Anisotropic scaling and a bulk solvent correction were used, and individual B atomic factors were refined anisotropically. Before a last refinement step, solvent molecules were added according to unassigned peaks in an F_o-F_cFourier difference map contoured at 2.5 σ. The final models consist of residues 229–458, the ligands, and 243 (for DHA) or 199 (for BMS 649) water molecules. In both structures, the H1–H3 connecting region and the last four amino acids are not visible.

For the triclinic form, molecular replacement calculations were carried out between 30 and 3.5 Å using the structure solved with the tetragonal crystals. Both monomeric and homodimeric models yielded unambiguous solutions. The

refinement was initially carried out in the 30–2.6 Å resolution range and then extended to 1.9 Å resolution. The quality of the density maps allowed us to reliably build a highly structured portion of the H1–H3 loop in only two of the four monomers. Initially, each monomer was successively fixed during the refinement, and restrained noncrystallographic constraints were applied to the helical parts of the structure; at the last cycle of refinement, noncrystallographic symmetry constraints were removed, and all four monomers were refined simultaneously. Anisotropic scaling and a bulk solvent correction were used and individual B atomic factors were refined anisotropically. Before the last refinement step, solvent molecules were added according to unassigned peaks in an F_o-F_cFourier difference map contoured at 2.5 σ. The final model contains 829 water molecules and four monomers consisting of residues 229–458 and the ligand.

According to PROCHECK (57), 94% of all residues in all models are in the most allowed main-chain torsion angle Ramachandran regions and 6% in the additionally allowed regions.

Acknowledgments

We are grateful to Drs. Giuseppe Tocchini-Valentini and Valérie Lamour for useful suggestions and help with the generation of the parameter and topology files for the ligands. We wish to thank Julien Lescar, our local contact at European Synchrotron Radiation Facility, Gilbert Bey, and Denis Zeyer for help during data collection. We thank Jean-Paul Renaud for critical reading of the manuscript and Souphatta Sasorith for advice with volume calculations.

Received August 15, 2001. Accepted December 21, 2001.

Address all correspondence and requests for reprints to: Dino Moras, Laboratoire de Biologie et Genomique Structurales, Institut de Genetique et Biologie Moleculaire et Cellulaire, Centre National de la Recherche Scientifique/Institut National de la Santé et de la Recherche Médicale/Université Louis Pasteur, Parc d'Innovation BP163, 1 rue Laurent Fries, 67404 Illkirch cedex, France. E-mail: moras@igbmc.u-strasbg.fr.

This work was supported by the Université Louis Pasteur de Strasbourg, the Centre National de la Recherche Scientifique, the Institut National de la Santé et de la Recherche Médicale and Bristol-Myers-Squibb. P.F.E. was the recipient of a fellowship from Association pour la Recherche sur le Cancer.

* Present adress: Macromolecular Structure Group, University of California San Francisco, Department of Biochemistry and Biophysics, School of Medicine, 513 Parnassus Avenue, Box 0448, San Francisco, California 94143.

REFERENCES

1. Gronemeyer H, Laudet V 1995 Transcription factors 3: nuclear receptors. Protein Profile 2:1173–1308
2. Steinmetz AC, Renaud JP, Moras D 2001 Binding of ligands and activation of transcription by nuclear receptors. Annu Rev Biophys Biomol Struct 30:329–359
3. Weatherman RV, Fletterick RJ, Scanlan TS 1999 Nuclear-receptor ligands and ligand-binding domains. Annu Rev Biochem 68:559–581
4. Egea PF, Klaholz BP, Moras D 2000 Ligand-protein interactions in nuclear receptors of hormones. FEBS Lett 476:62–67
5. Kastner P, Mark M, Chambon P 1995 Nonsteroid nuclear receptors: what are genetic studies telling us about their roles in real life? Cell 83:859–869
6. Chambon P 1996 A decade of molecular biology of retinoic acid receptors. FASEB J 10:940–954
7. Heyman RA, Mangelsdörf DJ, Dyck JA, Stein RB, Eichele G, Evans RM, Thaller C 1992 9-*cis*-Retinoic acid is a high affinity ligand for the retinoid X receptor. Cell 68:397–406
8. Levin AA, Sturzenbecker LJ, Kazmer S, Bosakowski T, Huselton C, Allenby G, Speck J, Kratzeisen C, Rosenberger M, Lovey A 1992 9-*cis*-Stereoisomer of retinoic acid binds and activates the nuclear receptor RXRα. Nature 355:359–361
9. Allegretto EA, McClurg MR, Lazarchik SB, Clemm DL, Kerner SA, Elgort MG, Boehm MF, White SK, Pike JW, Heyman RA 1993 Transactivation properties of retinoic acid and retinoid X receptors in mammalian cells and yeast. J Biol Chem 268:26625–26633
10. Allenby G, Bocquel M-T, Saunders M, Kazmer S, Speck J, Rosenberger M, Lovey A, Kastner P, Grippo J, Chambon P 1993 Retinoic acid receptors and retinoid X receptors: interactions with endogenous retinoic acid. Biochemistry 90:30–34
11. Egea PF, Mitschler A, Rochel N, Ruff M, Chambon P, Moras D 2000 Crystal structure of the human RXRα ligand-binding domain bound to its natural ligand: 9-*cis*-retinoic acid. EMBO J 19:2592–2601
12. Gampe RT, Montana VG, Lambert MH, Miller AB, Bledsoe RK, Milburn MV, Kliewer SA, Willson TM, Xu E 2000 Asymmetry in the PPARγ/RXRαcrystal structure reveals the molecular basis of heterodimerization among nuclear receptors. Mol Cell 5:545–555
13. Willy PJ, Mangelsdörf DJ 1997 Nuclear orphans receptors: the search for novel ligands and signalling pathways. In: O'Malley B, ed. Hormones and signaling. New York: Academic Press; 307–358
14. Mangelsdörf DJ, Evans RM 1995 The RXR heterodimers and orphans receptors. Cell 83:841–850
15. Kersten S, Reczek PR, Noy N 1997 The tetramerization region of the retinoid X receptor is important for transcriptional activation by the receptor. J Biol Chem 272: 29759–29768
16. Gampe RT, Montana VG, Lambert MH, Wisely GB, Milburn MV, Xu EH 2000 Structural basis for autorepression of retinoid X receptor by tetramer formation and the AF-2 helix. Genes Dev 14:2229–2241
17. Egea PF, Rochel N, Birck C, Vachette P, Timmins PA, Moras D 2001 Effects of ligand binding on the association properties and conformation in solution of retinoic acid receptors RXR and RAR. J Mol Biol 307:557–576
18. Laudet V 1997 Evolution of the nuclear receptor superfamily: early diversification from an ancestral orphan receptor. J Mol Endocrinol 19:207–226
19. Oro AE, McKeown MK, Evans RM 1990 Relationship between the product of the *Drosophila* ultraspiracle locus and the vertebrate retinoid X receptor. Nature 347: 298–301
20. Jones GA, Sharp PA 1997 Ultraspiracle: an invertebrate nuclear receptor for juvenile hormones. Proc Natl Acad Sci USA 94:13499–13503
21. Billas IML, Moulinier L, Rochel N, Moras D 2001 Crystal structure of the ligand-binding domain of the ultraspiracle protein USP, the ortholog of retinoid X receptors in insects. J Biol Chem 10:7465–7474
22. Clayton GM, Peak-Chew SY, Evans RM, Schwabe JWR 2001 The structure of the ultraspiracle ligand-binding domain reveals a nuclear receptor locked in an inactive conformation. Proc Natl Acad Sci USA 98:1549–1554
23. Escriva H, Delaunay F, Laudet V 2000 Ligand binding and nuclear receptor evolution. Bioessays 22:717–727
24. Mangelsdörf DJ, Umesono K, Evans RM 1994 The retinoids. In: Sporn MB, Roberts AB, Goodman DS, eds. Biology, chemistry, and medicine. New York: Raven Press Ltd.; 319–349
25. Parker RS 1996 Absorption, metabolism, and transport of carotenoids. FASEB J 10:542–551

26. Bourguet W, Vivat V, Wurtz, J-M, Chambon P, Gronemeyer H, Moras D 2000 Crystal structure of a heterodimeric complex of RAR and RXR ligand-binding domains. Mol Cell 5:289–298
27. Mata de Urquiza A, Liu S, Sjöberg M, Zetterström RH, Griffiths W, Sjövall J, Perlmann T 2000 Docosahexaenoic acid, a ligand for the retinoid X receptor in mouse brain. Science 290:2140–2144
28. Bischoff ED, Gottardis MM, Moon TE, Heyman RA, Lamph WW 1998 Beyond tamoxifen: the retinoid X receptor selective ligand LGD 1069 (Targretin) causes complete regression of mammary carcinoma. Cancer Res 58:479–484
29. Wurtz J-M, Bourguet W, Renaud J-P, Vivat V, Chambon P, Moras D, Gronemeyer H 1996 A canonical structure for the ligand-binding domain of nuclear receptors. Nat Struct Biol 3:87–94
30. Shiau AK, Barstad D, Loria PM, Cheng L, Kushner PJ, Agard DA, Greene GL 1998 The structural basis of estrogen receptor/coactivator recognition and the antagonism of this interaction by tamoxifen. Cell 95:927–937
31. Darimont BD, Wagner RL, Apriletti JW, Stallcup MR, Kushner PJ, Baxter JD, Fletterick RJ, Yamamoto KR 1998 Structure and specificity of nuclear receptor-coactivator interactions. Genes Dev 12:3343–3356
32. Nolte RT, Wisely GB, Westin S, Cobb JE, Lambert MH, Kurokawa R, Rosenfeld MG, Willson TM, Glass CK, Millburn MV 1998 Ligand binding and coactivator assembly of peroxysome proliferator activated receptor γ. Nature 395:137–143
33. Bourguet W, Ruff M, Chambon P, Gronemeyer H, Moras, D 1995 Crystal structure of the ligand binding domain of the human nuclear receptor RXRα. Nature 375:377–382
34. Rochel N, Tocchini-Valentini G, Egea PF, Juntunen K, Garnier J-M, Vihko P, Moras D 2001 Biochemical and biophysical characterization of the ligand binding domain of the vitamin D nuclear receptor. Eur J Biochem 268: 971–979
35. Egea PF, Moras D 2001 Purification and crystallization of human RXRαligand binding domain/9-*cis*-retinoic acid complex. Acta Crystallogr D 57:434–437
36. Klaholz BP, Moras D 2000 Structural role of a detergent molecule in retinoic acid nuclear receptor crystals. Acta Crystallogr D 56:933–935
37. Stehlin C, Wurtz J-M, Steinmetz A, Greiner E, Schuele R, Moras D, Renaud J-P 2001 X-ray structure of the orphan nuclear receptor RORβ ligand-binding domain in the active conformation. EMBO J 20–21:5822–5831
38. Harmon MA, Boehm MF, Heyman RA, Mangelsdörf DJ 1995 Activation of mammalian retinoid X receptor by the insect growth regulator methoprene. Proc Natl Acad Sci USA 92:6157–6160
39. Kitareewan S, Burka L, Tomer B, Parker CE, Deterding LJ, Stevens, RD, Forman BM, Mais DE, Heyman RA, McMorris T, Weinberger C 1996 Phytol metabolites are circulating dietary factors that activate the nuclear receptor RXR. Mol Cell Biol 7:1153–1166
40. LeMotte PK, Keidek S, Apfel CM 1996 Phytanic acid is a retinoid X receptor ligand. Eur J Biochem 236:328–333
41. Yu K, Bayona W, Kallen CB, Harding HP, Ravera CP, McMahon G, Brown M, Lazar MA 1995 Differential activation of peroxisome proliferator-activated receptors by eicosanoids. J Biol Chem 270:23975–23983
42. Devchand PR, Keller H, Peters JM, Vazquez M, Gonzalez FJ, Wahli W 1996 The PPARα-leukotriene B_4 pathway to inflammation control. Nature 384:39–43
43. Kliewer SA, Lenhard JM, Wilson TM, Patel I, Morris DC, Lhman JM 1995 A prostaglandin J_2metabolite binds peroxisome proliferator-activated receptor γ and promotes adipocyte differentiation. Cell 83:813–819
44. Forman BM, Tontonoz P, Chen J, Brun RP, Spiegelman BM, Evans RM 1995 15 Deoxy Δ,14 prostaglandin J_2 is a ligand for the adipocyte determination fatcor PPARγ. Cell 83:803–812
45. Xu EH, Lambert MH, Montana VG, Parks DJ, Blanchard SG, Brown PJ, Sterrmbach DD, Lehman JM, Wisely GB, Willson TM, Kmiewer SA, Milburn MV 1999 Molecular recognition of fatty acids by peroxysome proliferator-activated receptors. Mol Cell 3:397–403
46. Vivat V, Zechel C, Wurtz J-M, Bourguet W, Kagechika H, Umemiya H, Shudo K, Moras D, Gronemeyer H, Chambon P 1997 A mutation mimicking ligand-induced conformational change yields a constitutive RXR that senses allosteric effects in heterodimers. EMBO J 16:5697–5709
47. Peet DJ, Doyle DF, Corey DR, Mangelsdörf DJ 1998 Engineering novel specificities for ligand-activated transcription in the nuclear hormone receptor RXR. Chem Biol 5:13–21
48. Tocchini-Valentini G, Rochel N, Wurtz J-M, Mitschler A, Moras D 2001 Crystal structures of the vitamin D receptor complexed to super agonist 20-epi ligands. Proc Natl Acad Sci 98:5491–5496
49. Klaholz BP, Renaud J-P, Mitschler A, Zusi C, Chambon P, Gronemeyer H, Moras D 1998 Conformational adaptation of agonists to the human nuclear receptor RARγ. Nat Struct Biol 5:199–201
50. Klaholz BP, Mitschler A, Belema M, Moras D 2000 Enantiomer discrimination illustrated by high-resolution crystal structures of the human nuclear receptor hRARγ. Proc Natl Acad Sci USA 97:6322–6327
51. Hong L, Zhang XC, Harstuck JA, Tang J 2000 Crystal structure of an *in vivo* HIV-1 protease inhibitor in complex with saquinavir: insights into the mechanism of drug resistance. Protein Sci 9:1898–1904
52. Boden D, Markowitz M 1998 Resistance to human immunodeficiency virus type 1 protease inhibitors. Antimicrob Agents Chemother 42:2775–2783
53. Otwinowski Z, Minor W 1996 Processing x-ray data collected in oscillation mode. Methods Enzymol 276: 307–326
54. Navaza, J 1994 *AmoRe*: an automated package for molecular replacement. Acta Crystallogr A 50:157–163
55. Brünger AT, Adams PD, Clore GM, DeLano WL, Gros P, Grosse-Kunstleve RW, Jiang JS, Kuszewski J, Nilges M, Pannu NS, Read RJ, Rice LM, Simonson T, Warren GL 1998 Crystallography & NMR system: a new software suite for macromolecular structure determination. Acta Crystallogr D 54:905–921
56. Jones TA, Zou JY, Cowan SW, Kjeldgaard M 1991 Improved methods for building proteins models in electron density maps and the location of errors in these models. Acta Crystallogr A 47:110–119
57. Laskowski RA, MacArthur MW, Moss DS, Thornton JM 1993 *PROCHECK*: a program to check the stereochemical quality of protein structure coordinates. J Appl Crystallogr 26:283–291
58. Kleywegt G, Jones TA 1994 Detection, delineation, measurement and display of cavities in macromolecular structures. Acta Crystallogr D 50:178–185
59. Philippsen A 1999 *DINO*: visualizing structural biology. http://www.bioz.unibas.ch/~xray/dino